Effects of collision energy and vibrational excitation of CH_3^+ cations on its reactivity with hydrocarbons: But-2-yne CH_3CCCH_3 as reagent partner

Andrea Cernuto, Allan Lopes, Claire Romanzin, Barbara Cunha de Miranda, Daniela Ascenzi, Paolo Tosi, Glauco Tonachini, Andrea Maranzana, Miroslav Polášek, Jan Žabka, and Christian Alcaraz

Citation: The Journal of Chemical Physics **147**, 154302 (2017);

View online: https://doi.org/10.1063/1.4990514

View Table of Contents: http://aip.scitation.org/toc/jcp/147/15

Published by the American Institute of Physics

Effects of collision energy and vibrational excitation of CH_3^+ cations on its reactivity with hydrocarbons: But-2-yne CH_3CCCH_3 as reagent partner

Andrea Cernuto,[1] Allan Lopes,[2] Claire Romanzin,[2,3] Barbara Cunha de Miranda,[3,4] Daniela Ascenzi,[1,a)] Paolo Tosi,[1] Glauco Tonachini,[5] Andrea Maranzana,[5] Miroslav Polášek,[6] Jan Žabka,[6] and Christian Alcaraz[2,3]

[1]*Department of Physics, University of Trento, Via Sommarive 14, Trento I-38123, Italy*
[2]*Laboratoire de Chimie Physique, Bât. 350, UMR 8000, CNRS-Univ. Paris-Sud 11 and Paris Saclay, Centre Universitaire Paris-Sud, 91405 Orsay Cedex, France*
[3]*Synchrotron SOLEIL, L'Orme des Merisiers, Saint-Aubin – BP 48, 91192 Gif-sur-Yvette, France*
[4]*Sorbonne Université, UPMC Université Paris 06, CNRS, UMR 7614, Laboratoire de Chimie Physique-Matiére et Rayonnement, F-75005 Paris, France*
[5]*Department of Chemistry, University of Torino, Via Pietro Giuria, 7, Torino I-10125, Italy*
[6]*J. Heyrovský Institute of Physical Chemistry of the Czech Academy of Sciences, Dolejškova 3, 182 23 Prague 8, Czech Republic*

(Received 15 June 2017; accepted 25 September 2017; published online 16 October 2017)

The methyl carbocation is ubiquitous in gaseous environments, such as planetary ionospheres, cometary comae, and the interstellar medium, as well as combustion systems and plasma setups for technological applications. Here we report on a joint experimental and theoretical study on the mechanism of the reaction $CH_3^+ + CH_3CCCH_3$ (but-2-yne, also known as dimethylacetylene), by combining guided ion beam mass spectrometry experiments with *ab initio* calculations of the potential energy hypersurface. Such a reaction is relevant in understanding the chemical evolution of Saturn's largest satellite, Titan. Two complementary setups have been used: in one case, methyl cations are generated via electron ionization, while in the other case, direct vacuum ultraviolet photoionization with synchrotron radiation of methyl radicals is used to study internal energy effects on the reactivity. Absolute reactive cross sections have been measured as a function of collision energy, and product branching ratios have been derived. The two most abundant products result from electron and hydride transfer, occurring via direct and barrierless mechanisms, while other channels are initiated by the electrophilic addition of the methyl cation to the triple bond of but-2-yne. Among the minor channels, special relevance is placed on the formation of $C_5H_7^+$, stemming from H_2 loss from the addition complex. This is the only observed condensation product with the formation of new C—C bonds, and it might represent a viable pathway for the synthesis of complex organic species in astronomical environments and laboratory plasmas. *Published by AIP Publishing.* https://doi.org/10.1063/1.4990514

I. INTRODUCTION

The methyl carbocation (or methylium), the simplest among carbenium ions, is one of the most important reactive intermediates in solution phase organic chemistry, having a high chemical and biological activity due its strong electrophilic character.[1–3]

In the gas phase, the methyl cation is ubiquitous in environments fed by high energy sources, and it is an especially important molecular ion in combustion systems and plasma setups for technological applications. CH_3^+ is thought to be present in methane flames[4,5] and, more importantly, in laboratory plasmas, with a particular reference to those used for methane conversion into higher hydrocarbons[6] or plasma-based dry reforming of CO_2/CH_4 mixtures, i.e., their conversion into value-added chemicals.[7,8] Methylium ions are also typical of astrophysical plasmas, ranging from the various regions of the interstellar medium (ISM) to planetary atmospheres, cometary comae, etc. In the ISM, where methyl cation abundances are inferred by the detection of its singly deuterated counterpart CH_2D^+, CH_3^+ plays a central role in the organic chemistry of dense and diffuse interstellar clouds, where it may be held responsible for the synthesis of methane and more complex hydrocarbons, according to the various chemical models proposed for the composition of different regions of the ISM.[9–15] Although the role of the methyl cation in chemistry of cold clouds via radiative association with H_2 and subsequent dissociative electron recombination of the CH_5^+ cation[16,17] has been questioned,[18,19] the reactions of CH_3^+ with simple molecules (not only H_2 but also NH_3, H_2O, HCN, and CH_3OH) need to be included to model the chemistry of portions of clouds at elevated temperatures, such as hot cores, or inner regions of protoplanetary disks.[20]

Methyl cation has been detected to be an important ion in the innermost coma of comet Halley,[21] in the ionosphere

a)daniela.ascenzi@unitn.it

of Jupiter[22] and Saturn,[23] and in the atmosphere of Titan, Saturn's largest moon, as demonstrated by the Cassini-Huygens mission.[24–31] We can speculate that methyl cations may be present in the atmospheres of planets beyond the boundaries of our Solar System, where the number of newly discovered extrasolar planets has increased by two orders of magnitude in the last two decades.[32] Amazingly, some of the detected exoplanets are expected to be C-rich and contain a high quantity of methane and heavier hydrocarbons,[33–40] thus making the formation of the CH_3^+ ion feasible and its reactivity relevant for shaping the chemistry and composition of exoplanets.

On Titan, CH_3^+ is present at intermediate quantities[41–43] as a secondary product of the ion and neutral chemistry. In fact, it is produced by photoionization and electron impact dissociation and ionization of CH_4, as well as from the reactions of N_2^+ and N^+ with CH_4.[44,45] CH_3^+ is a key ion in the chemical models for Titan's upper atmosphere since, by reaction with CH_4, it leads to the formation of $C_2H_5^+$, one of the most abundant ions detected in Titan's ionosphere, and subsequently to ethylene C_2H_4 and acetylene C_2H_2, thus opening the way to the formation of a series of complex hydrocarbons.[25,45] Quite relevant for understanding the chemical evolution of Titan's atmosphere is the study of the reactivity of CH_3^+ with methyl substituted acetylenes [i.e., propyne C_3H_4, an abundant molecule in Titan's thermosphere and ionosphere, and but-2-yne (C_4H_6)]. Such reactions have been recently suggested[46] to be responsible for the couples of ions ($C_4H_7^+/C_4H_5^+$ and $C_5H_9^+/C_5H_7^+$) observed by the ion neutral mass spectrometer on board of the Cassini probe.[28,43]

Methyl carbocations are expected to react via electrophilic ion-neutral reactions with both unsaturated and saturated hydrocarbons. In the former case, a π-electron pair from unsaturated hydrocarbons is donated to the electrophile via the formation of a three-center two-electron bond, while in the latter case, donation of electrons in sigma bonds can play a role in the formation of products via complexes having non-classical structures and delocalized three-center bonds. The reactions of methyl carbocations with simple hydrocarbons (methane,[47,48] ethane,[49–52] propane,[49] ethene, and ethyne[52–56]) have been investigated, by a variety of experimental techniques and theoretical calculations, since the very early days of gas-phase ion chemistry.

This paper presents an experimental study of the reactivity of methyl cations with but-2-yne (C_4H_6) by measuring absolute reactive cross sections and branching ratios (BRs) as a function of collision energy using two different guided ion beam setups, as well as a theoretical investigation of possible reaction pathways using *ab initio* calculations. While in one setup, the methyl cation is generated with an uncontrolled amount of internal excitation using an electron ionization (EI) source, in the other setup, direct vacuum ultraviolet (VUV) photoionization with synchrotron radiation of methyl radicals is used to produce CH_3^+. This alternative generation method allows the production of the methyl cation with a controlled amount of internal excitation, as described in the companion paper about the reaction of CH_3^+ ions with methane,[57] thus opening the possibility to investigate the effect of internal degrees of freedom (electronic and vibrational) on the reactivity, a subject of extreme interest for the modeling of high energy environments where the populations of excited states of ions can be non-negligible.

II. EXPERIMENTAL METHODS

The reaction of methyl cation CH_3^+ with but-2-yne (C_4H_6) has been investigated by using both the home-built Guided-Ion Beam Mass Spectrometer (GIB-MS) at Trento (Italy) and the CERISES-apparatus,[57,58] a GIB-MS apparatus of the LCP laboratory at Orsay installed for these experiments on the DESIRS beamline of the synchrotron radiation source SOLEIL (St. Aubin, France).

A. The Trento GIB-MS setup

The Trento GIB setup was described previously[59–61] and therefore only a brief summary is here reported. It consists of a tandem mass spectrometer with an O1-Q1-O2-Q2 configuration (where Q stands for quadrupole and O stands for octopole). Methyl ions are generated by dissociative electron ionization (EI) of acetone at energies in the range 45 eV–55 eV. The first octopole O1 is operated as an ion guide, while CH_3^+ ions are mass selected by quadrupole Q1 before being injected into octopole O2, which is surrounded by the scattering cell filled with the neutral reactant, the pressure of which is monitored by a spinning rotor gauge (SRG2 MKS Instruments, MA USA). The effective length of the scattering cell is 12.0(6) cm. In the present case, the cell is filled with gaseous but-2-yne at variable pressures in the range 6.0×10^{-7} mbar to 7.0×10^{-4} mbar. The but-2-yne liquid sample (SIGMA-ALDRICH 99%) was degassed by repeated freeze-pump-thaw cycles before injection, and it was kept at a temperature in the range 250 K–260 K using a water/ice/NaCl bath.

The kinetic energy of the projectile ion beam in the laboratory frame, which determines the collision energy, can be varied from practically 0 to several tens of eV by changing the dc bias potential of O2. Laboratory frame collision energies, E_{LAB}, are converted to the corresponding values in the center-of-mass (CM) frame, E_{CM}, via the formula

$$E_{CM} = \frac{m}{M+m} \cdot E_{LAB},$$

where m and M stand for the mass of the neutral target and the ionic projectile, respectively. Product ions are mass analysed by Q2 and detected by an electron multiplier. The ratio between the measured signal intensities of product and reactant ions is proportional to the effective integral cross section according to the Lambert-Beer law,[62] and the absolute value of the cross section can be obtained by measuring the ratio of product and reactant ion intensities as a function of the neutral gas density, at sufficiently low pressures of the neutral reactants to ensure a single collision regime within the scattering cell.

B. The CERISES setup @ DESIRS beamline, SOLEIL synchrotron

As the CERISES apparatus is described in detail in previous papers[58,63] and the companion paper,[57] only the most important points are recalled here. CERISES is a guided ion

beam tandem mass spectrometer composed of two octopoles located between two quadrupole mass spectrometers in a Q1-O1-O2-Q2 configuration that permits the investigation of bi-molecular reactions of mass-selected ions, by measuring parent and product ion yields from which absolute reaction cross sections, BRs, and product velocity distributions as a function of collision energies and photon energy are derived.[58,63]

The setup has been recently modified[57] with the addition of a molecular beam chamber to produce hydrocarbon radicals by flash-pyrolysis of organic precursors. In this work, the $CH_3^\bullet$ radical is produced using CH_3NO_2 as a precursor in an Ar seeded molecular beam. The $CH_3^\bullet$ radical is subsequently photo-ionised with the VUV radiation from the DESIRS beamline and its cations transferred into the reactive part of CERISES. The internal excitation of the parent cation can be varied by changing the photon energy from the threshold ionization of $CH_3^\bullet$ (about 9.8 eV) to 12.5 eV. This last limit prevents from any contamination by CH_3^+ ions that could arise from dissociative ionization of partially pyrolysed nitromethane precursors, as shown in a previous study using the same pyrolysis source.[64] The distribution of the CH_3^+ vibrational excitation and hence its mean value have been measured in a separate experiment as a function of photon energy.[57] The undulator based DESIRS beamline[65] provides tunable radiation in the vacuum ultraviolet (VUV) range from about 5 eV to 40 eV. Photons at the desired wavelength are selected and scanned simultaneously with the undulator peak energy by a normal incidence monochromator equipped with a low dispersion uncoated SiC grating (200 grooves mm^{-1}) optimised to provide photon flux in the 10^{12} photon/s–10^{13} photon/s range with a moderate energy resolution in the 5 eV–20 eV range. In the present experiments, the monochromator exit slits were opened to 600 μm, which delivers a photon energy bandwidth of about 52 meV at a photon energy of 12 eV. Second order light from the undulator was completely removed by an upstream gas filter filled with Ar at about 0.2 mbar.[66] The photon energy was calibrated by measuring the ionization energy of CH_3 around 9.839 eV[67] and the two strong absorption lines of Ar $3s^23p^6(^1S_0) \rightarrow 3s^23p^5(^2P_{3/2})4s^2\ [3/2]_1$ and $3s^23p^6(^1S_0) \rightarrow 3s^23p^5(^2P_{1/2})4s^2\ [1/2]_1$ at 11.624 eV and 11.828 eV, respectively.[68]

For the ion-molecule reaction experiments, the CH_3^+ reagent ions were mass-selected using Q1 and focused into the O1 radio frequency guide terminated by a 4 cm long scattering cell filled with the target gas (but-2-yne in our case) at room temperature. A Baratron capacitance manometer measured the absolute value of the neutral gas pressure, adjusted to values of about 1×10^{-4} mbar and 2×10^{-4} mbar to ensure single-collision conditions. The reactant ion kinetic energy, defined by the dc potential difference between O1 and the center of the ion source, can be varied between practically zero and 20 eV in the laboratory energy frame. The typical distribution width is in the range 0.7 eV–0.8 eV full width at half maximum (FWHM), leading to a collision energy in the CM frame up to 8 eV, with a width of about 0.55 eV–0.62 eV (FWHM). Reactant and product ions were confined by the radio-frequency field of O1, guided by O2, mass selected in the Q2 mass filter, and finally detected by a multi-channel plate operating in the counting mode. For the reactive-monitoring experiments, Q1 was set to mass-select the CH_3^+ parent, Q2 was set to the mass-to-charge ratio of the parent or product ion, and the photon energy was scanned in steps of 20 meV, while keeping all the other experimental parameters (neutral gas pressure, collision energy, focusing ion optics potentials, etc.) fixed. During the measurement of the ion yields, also photon fluxes were simultaneously recorded by photoemission currents from a gold grid, and the raw data for the measured ion yields were accordingly corrected for the photon flux of the beamline as a function of the photon energy.[69] From the ratio of product to parent ion yields and the neutral target pressure measurement, the absolute reaction cross sections are derived following standard procedures.

III. THEORETICAL METHODS

All stationary points on the potential energy hypersurface, i.e., minima and first order saddle points, corresponding to transition states (TS), were determined within the Density Functional Theory (DFT),[70] making use of the M06-2X[71–74] functional with the cc-pVTZ basis set.[75] The nature of the critical points was checked by the vibrational analysis. The optimizations were followed by CCSD(T) [Coupled Cluster theory with Single, Double and (non-iteratively) Triple excitations] single-point energy computations, with the cc-pVTZ[75] and cc-pVQZ[76] basis sets, to finally obtain CCSD(T)/CBS (complete basis set) energy estimates. The use of DFT for geometry optimization is a standard procedure commonly adopted in the theoretical chemistry community (see recent examples dealing with hydrocarbon cations[77–79]). Its choice is dictated by the fact that optimizations at the CCSD(T) level of theory are computationally very demanding and at the limit of feasibility for the systems under study.

The total CBS energy (E^∞) is the sum of the Hartree-Fock energy and correlation energy, which are extrapolated separately,

$$E^\infty = E^\infty_{H-F} + E^\infty_{corr}.$$

For the correlation energy, the two-parameter extrapolation formula proposed by Halkier *et al.*[80] was used,

$$E^\infty_{corr} = \frac{E^{corr}_X X^3 - E^{corr}_Y Y^3}{X^3 - Y^3}.$$

The energy estimate $E_{X,Y}$ exploits the energies obtained with the two basis sets cc-pVXZ and cc-pVYZ (E_X and E_Y, respectively). In this study, $X = 3$ and $Y = 4$, and the two-point formula was thus simply used as

$$E^\infty_{3,4} = \frac{E_3 3^3 - E_4 4^3}{3^3 - 4^3}.$$

For the Hartree-Fock part, the CBS energy was estimated by using the two-point exponential extrapolation formula[81]

$$E^{H-F}_X = E^\infty_{H-F} + Be^{-\alpha X},$$

where the empirical parameter α was kept fixed ($\alpha = 1.63$),[81] X was the cardinal number of the basis set cc-pVXZ, and the two parameters B and E^∞_{H-F} were obtained fitting the sets of data.

The M06-2X/cc-pVTZ thermochemical corrections gave estimates of the zero-point vibrational energy, by which the energies were corrected to obtain $\Delta E_{ZPE}[= \Delta(E + ZPE)]$ values. These ΔE_{ZPE} values at CCSD(T)/CBS are reported throughout in the text. Geometry optimizations and thermochemistry calculations were carried out by using the GAUSSIAN 09 system of programs.[82] Geometries and energetics of all the optimised structures are reported in the supplementary material. The Molden package has been used for the visualisation of molecular structures.[83]

IV. EXPERIMENTAL RESULTS

A. GIB-MS at the University of Trento

A mass spectrum of the ionic products for the reaction of CH_3^+ with but-2-yne (C_4H_6), recorded with the Trento GIB-MS apparatus (EI source), is reported in Fig. 1. The spectrum was measured at a collision energy in the CM frame E_{CM} of about 0.2 eV and with a pressure of but-2-yne inside the reaction octopole of about 1.2×10^{-6} mbar to minimise the number of secondary collisions. The two most abundant ionic products are observed at *m/z* 53 and 54. For the former, a possible pathway might be an H^- abstraction by the methyl cation from the neutral compound to give the $C_4H_5^+$ ion via reaction (1), while the latter results from the charge transfer process, reaction (2). Another product ion with a large yield is $C_3H_5^+$ (*m/z* 41), which can exist in two different isomers (allyl and 2-propenyl[84]), and might be formed (together with a C_2H_4 counter-fragment) by the electrophilic addition of CH_3^+ to the triple bond of C_4H_6 via channels (3a) and (3b),

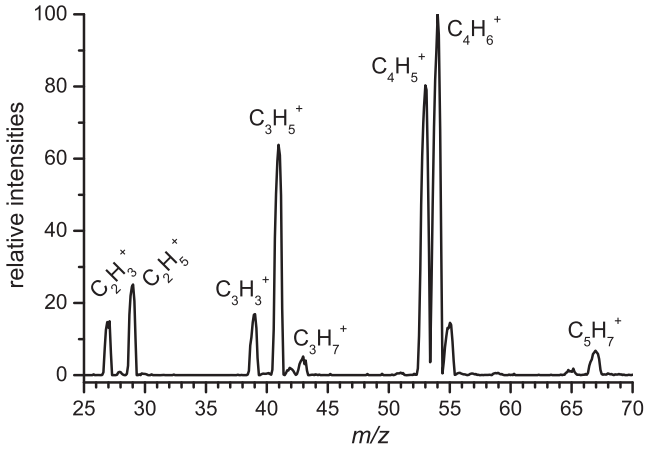

FIG. 1. Typical mass spectrum of ionic products from mass selected CH_3^+ ions reacting with but-2-yne, recorded at a collision energy in the CM frame $E_{CM} \sim 0.2$ eV and with $\sim 1.2 \times 10^{-6}$ mbar of but-2-yne in the reaction cell. The intensities are normalized to the most abundant product ion (set at 100).

$$CH_3^+ + C_4H_6 \longrightarrow C_4H_5^+ (m/z\ 53) + CH_4 \quad (1)$$

$$\longrightarrow C_4H_6^{\bullet +} (m/z\ 54) + CH_3 \quad (2)$$

$$\longrightarrow C_3H_5^+ (m/z\ 41)\ [\text{allyl}] + C_2H_4 \quad (3a)$$

$$\longrightarrow C_3H_5^+ (m/z\ 41)\ [\text{2-propenyl}] + C_2H_4\ . \quad (3b)$$

Other ions are observed in smaller yields and their appearance can be explained with some of the following processes:

$$CH_3^+ + C_4H_6 \longrightarrow C_2H_5^+ (m/z\ 29) + CH_3CCH\ /\ CH_2CCH_2 \quad (4a, 4b)$$

$$\longrightarrow c\text{–}C_3H_3^+ (m/z\ 39) + 2\ CH_3^{\bullet}\ /\ C_2H_6\ /\ C_2H_4 + H_2 \quad (5a, 5b, 5c)$$

$$\longrightarrow CH_2CCH^+ (m/z\ 39) + 2\ CH_3^{\bullet}\ /\ C_2H_6\ /\ C_2H_4 + H_2 \quad (5d, 5e, 5f)$$

$$\longrightarrow CH_2C(H)C^+ (m/z\ 39) + 2\ CH_3^{\bullet}\ /\ C_2H_6\ /\ C_2H_4 + H_2 \quad (5g, 5h, 5i)$$

$$\longrightarrow C_2H_3^+ (m/z\ 27) + C_2H_2 + CH_4\ /\ c\text{–}C_3H_6\ /\ C_3H_6 \quad (6a, 6b, 6c)$$

$$\longrightarrow C_5H_7^+ (m/z\ 67) + H_2 \quad (7)$$

$$\longrightarrow C_3H_7^+ (m/z\ 43) + C_2H_2\ . \quad (8)$$

The formation mechanisms for these channels will be discussed in Sec. V, where experimental results are interpreted in light of the potential energy hypersurface obtained from computational methods. However, it is useful to anticipate here the results for the reaction enthalpies ($\Delta_r H^\circ$) for channels (1)–(8): In Table I, a comparison is presented between reaction enthalpies estimated using experimental values for the standard heat of formations of reagents and products ($\Delta_f H^\circ$) and our calculated values for $\Delta_r H^\circ$ and $\Delta_r E_{ZPE}$ at the CCSD(T)/CBS level of theory. To the best of our knowledge, there are no experimental $\Delta_f H^\circ$ values for $C_5H_7^+$ available in the literature. Hence the entry about the experimental $\Delta_r H^\circ$ is missing in the table.

BRs for the various ionic products have been derived from the mass spectra by integrating the areas below each mass peak. The BR values, reported in Table II, have been obtained by averaging 3 sets of mass spectra taken at a collision energy $E_{CM} \sim 0.2$ eV and at three different but-2-yne pressures in the range 6.4×10^{-7} mbar–3.2×10^{-6} mbar. BRs have been corrected for small contributions (not bigger than 10% of the total product ion intensities) coming from secondary collisions of abundant or highly reactive primary products, giving peaks at *m/z* 55, 91, and 93. The error bars on the BRs allow the small corrections for secondary reactions, and more details on the origin and corrections for such peaks are reported in the supplementary material.

TABLE I. Comparison between experimental and calculated reaction enthalpies $\Delta_r H^\circ$ at 298 K for product channels observed upon reaction of CH_3^+ with but-2-yne. Experimental $\Delta_r H^\circ$ are obtained from the experimentally determined heat of formations $\Delta_f H^\circ$ of reagents and products, while calculated ones refer to our calculations at the CCSD(T)/CBS level of theory.

m/z	Products	Equation	$\Delta_r H^\circ$ (eV)[a] Expt.	$\Delta_r H^\circ$ (eV) Calc	$\Delta_r E_{ZPE}$ (eV)[b] Calc
53	$[CH_3CCCH_2]^+ + CH_4$	(1)	−2.49[c]	−2.49	−2.48
54	$[CH_3CCCH_3]^{\bullet+} + CH_3^\bullet$	(2)	−0.26[d]	−0.28	−0.30
41	$[CH_2CHCH_2]^+$(allyl) + C_2H_4	(3a)	−2.56[e]	−2.45	−2.41
41	$[CH_2{=}CCH_3]^+$(2-propenyl) + C_2H_4	(3b)	−2.26[e]	−2.12	−2.10
29	$C_2H_5^+ + C_3H_4$ (propyne)	(4a)	−1.58[f]	−1.59	−1.55
29	$C_2H_5^+ + C_3H_4$ (allene)	(4b)	−1.54[f]	−1.55	−1.51
39	$[c{-}C_3H_3]^+ + 2\,CH_3^\bullet$	(5a)	+1.27[g]	+1.25	+1.21
39	$[c{-}C_3H_3]^+ + C_2H_6$	(5b)	−2.62[g]	−2.64	−2.59
39	$[c{-}C_3H_3]^+ + C_2H_4 + H_2$	(5c)	−1.21[g]	−1.20	−1.22
39	$[HCCCH_2]^+ + 2\,CH_3^\bullet$	(5d)	+2.35[g]	+2.49	+2.42
39	$[HCCCH_2]^+ + C_2H_6$	(5e)	−1.54[g]	−1.41	−1.38
39	$[HCCCH_2]^+ + C_2H_4 + H_2$	(5f)	−0.12[g]	+0.03	−0.01
39	$[CH_2{=}CHC{:}]^+ + 2\,CH_3^\bullet$	(5g)	+4.29[g]	+4.29	+4.23
39	$[CH_2{=}CHC{:}]^+ + C_2H_6$	(5h)	+0.40[g]	+0.40	+0.43
39	$[CH_2{=}CHC]^+ + C_2H_4 + H_2$	(5i)	+1.81[g]	+1.84	+1.80
27	$[CH_2CH]^+ + C_2H_2 + CH_4$	(6a)	+0.43[h]	+0.44	+0.39
27	$[CH_2CH]^+ + C_3H_6$ (cyclopropane)	(6b)	−0.59[h]	−0.58	−0.53
27	$[CH_2CH]^+ + C_3H_6$ (propene)	(6c)	−0.93[h]	−0.93	−0.91
67	$C_5H_7^+ + H_2$	(7)	n.a.	−2.51/−3.55	−2.51/−3.55[i]
43	$[(CH_3)_2CH]^+ + C_2H_2$	(8)	−2.0[j]	−2.19	−2.17

[a] $\Delta_f H^\circ$ reagents, used for all channels, are the following: $\Delta_f H^\circ$ (CH_3^+) = 11.35(2) eV[85] and $\Delta_f H^\circ$ (C_4H_6) = 1.50(1) eV.[85]

[b] $\Delta_r E_{ZPE}$ is the reaction ΔE_{ZPE} (see Sec. III).

[c] No experimental heat of formation value is available for the γ-methylpropargyl cation, so the calculated value $\Delta_f H^\circ(CH_3CCCH_2^+)$ = 11.14 eV is used from MP2/6-311G(d,p) calculations.[86]

[d] Obtained using $\Delta_f H^\circ(CH_3)$ = 1.51(1) eV[85] and $\Delta_f H^\circ(CH_3CCCH_3^{\bullet+})$ = 11.08(3) eV.[85]

[e] Obtained using $\Delta_f H^\circ$ = 9.75(10) eV for the allyl cation $CH_2CHCH_2^+$ and $\Delta_f H^\circ$ = 10.1(1) eV for the 2-propenyl cation $CH_3CCH_2^+$[84] in addition to $\Delta_f H^\circ$ (C_2H_4 ethylene) = 0.544(5) eV.[85]

[f] Obtained using $\Delta_f H^\circ$ ($C_2H_5^+$) = 9.35(3) eV,[84] $\Delta_f H^\circ$ (CH_3CCH) = 1.92(1) eV,[85] and $\Delta_f H^\circ$ (CH_2CCH_2) = 1.970(3) eV.[87]

[g] Obtained using $\Delta_f H^\circ$ = 11.1(1) eV for cyclopropenylium $c{-}C_3H_3^+$, $\Delta_f H^\circ$ = 12.19(6) eV for the propargyl cation CH_2CCH^+, and $\Delta_f H^\circ$ ($C_2H_5^+$) = 14.125 eV for the $CH_2C(H)C^+$ cation. The value for this latter ion comes from a theoretical estimate and it is therefore given with no error bar.[84]

[h] Obtained using $\Delta_f H^\circ$ (CH_2CH^+) = 11.71 eV from the theoretical estimate reported in Ref. 84.

[i] The two values refer to the production of two different $C_5H_7^+$ isomers, as it will be explained in Sec. V.

[j] Obtained using $\Delta_f H^\circ$ = 8.52(4) eV for the 2-propyl cation $[(CH_3)_2CH]^+$.[88] Note that this value is consistent with another experimental value $\Delta_f H^\circ$ = 8.48(4) eV from the work of Baer *et al.*[89]

Relative cross sections for channels reported in Table II have been measured as a function of collision energy, and results are shown in Fig. 2. The dependence of product ion abundances on the collision energy usually provides some insights into the reaction mechanisms. Usually, direct processes such as charge transfer, H transfer, or H^- transfer exhibit a small dependence on the collision energy, while complex-mediated exothermic processes having no significant energy barriers exhibit strongly decreasing dependencies of cross sections with increasing collision energy. Conversely, endothermic processes (or reactions with high energy barriers) require some excess energy to occur, hence cross sections are higher at higher collision energies.

TABLE II. Branching ratios for the formation of the main product channels observed upon reaction of CH_3^+ with but-2-yne. Data have been obtained by averaging 3 sets of mass spectra taken at a collision energy $E_{CM} \sim 0.2$ eV and three different but-2-yne pressures in the range 6.4×10^{-7} mbar–3.2×10^{-6} mbar.

m/z	Ion	Branching ratios (%)
27	$C_2H_3^+$	4.2 ± 0.7
29	$C_2H_5^+$	7.2 ± 2.0
39	$C_3H_3^+$	4.8 ± 1.0
41	$C_3H_5^+$	22.5 ± 4.6
43	$C_3H_7^+$	1.4 ± 0.7
53	$C_4H_5^+$	26.2 ± 4.2
54	$C_4H_6^{\bullet+}$	31.3 ± 5.2
67	$C_5H_7^+$	1.8 ± 0.3

It can be observed that some products (namely, $C_4H_5^+$, $C_3H_5^+$, $C_2H_5^+$, $C_5H_7^+$, and $C_3H_7^+$) exhibit decreasing values of the cross sections with the increase of the collision energy, thus speaking for exothermic processes presenting no energy barriers along the reaction path and/or processes occurring via the formation of a collision complex (these points will be discussed in detail in Sec. V), and are therefore compatible with channels (1), (3a), (3b), (4a), (4b), (7), and (8) of Table I.

On the other hand, $C_3H_3^+$ and $C_2H_3^+$ products show cross sections that are smallest at the lowest collision energies reachable with our setup and show an increasing trend

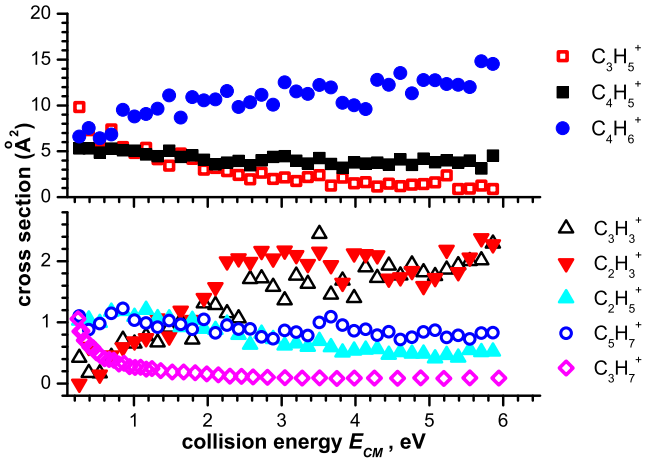

FIG. 2. Absolute cross sections for reactions (1)–(8) as a function of the collision energy E_{CM} for the reaction of mass-selected CH_3^+ with but-2-yne, measured using the Trento GIB-MS setup.

when the collision energy is increased. In Table I, channels from (5a)–(5i) relate to the formation of $C_3H_3^+$ [plus different counter-fragment(s)], which is known to exist in four isomeric structures: the cyclopropenyl cation (c-$C_3H_3^+$), the propargyl cation (CH_2CCH^+), $CH_2C(H)C^+$, and CH_3CC^+ (in the order of increasing energy). Only the three lowest energy isomers have been here considered since the formation of the CH_3CC^+ isomer would be too endothermic to be relevant in the present study. As for the neutral counter-fragment(s), three possibilities arise: (a) ethane (C_2H_6), which would give the most exothermic channels; (b) ethene (C_2H_4) plus H_2, and (c) formation of two methyl radicals ($CH_3^\bullet$), which would give the highest energy channels. The experimental findings of Fig. 2 are compatible with the occurrence of the slightly endothermic channels (5a) and (5h) or with the presence of barriers in the exothermic channels (5b), (5c), (5e), and (5f). Channels (5d), (5g), and (5i) can instead be excluded due to their too high endothermicities. For a detailed discussion of the most likely pathways for the production of $C_3H_3^+$, we refer to Sec. V.

In Table I, channels from (6a)–(6c) relate to the formation of the vinyl cation CH_2CH^+ plus different counter-fragment(s), namely, (a) ethyne (C_2H_2) plus CH_4, (b) C_3H_6 in the form of the cyclopropane isomer, and (c) C_3H_6 in the form of the propene isomer. While the formation of both C_3H_6 isomers are exothermic processes, channel (6a) is slightly endothermic and compatible with the experimental findings of Fig. 2. Also in this case, a detailed discussion of the most probable pathways for the production of $C_2H_3^+$ will be presented in Sec. V.

B. "CERISES" guided ion beam apparatus at SOLEIL synchrotron

The reaction of CH_3^+ with 2-butyne has been studied also using the *reaction monitoring technique* with synchrotron radiation. This technique has been amply used in previous studies[90–96] to sample the changes in ion reactivity induced upon ionization of a neutral precursor with photons of variable energies. In the experiment at SOLEIL, parent and product ion yields are monitored in the tandem mass spectrometer as a function of the energy of the ionizing photons (E_{phot}). It is fundamental to point out that, in such experiments, all parameters possibly affecting the reactivity or the yield of product ions (such as mass-selection, collision energy, neutral gas pressure in the reaction cell, collection optics) are kept constant while the ionizing photon energy is scanned.

For the eight product channels from reactions (1)–(8), experimental data in the reaction monitoring method are collected and analyzed in the following way: the primary and product ion intensities are recorded, at a fixed collision energy E_{CM} = 0.3 eV in the CM frame, as a function of the photon energy from 9.5 eV to 12.5 eV with a step of 0.05 eV, and from the ratio of product ion intensity over primary ion intensity, the absolute value of the cross sections is obtained using standard procedures. Note in passing that since the yields of product ions are normalized over the intensity of the CH_3^+ parent, results presented in this way are independent of the variation of the photon flux of the beamline as a function of the photon energy, hence normalization for the photon flux recorded by photoemission currents from a gold grid is not necessary.

Results for product ions at *m/z* 53 ($CH_3CCCH_2^+$), 54 ($CH_3CCCH_3^+$), and 41 ($C_3H_5^+$) are reported in Fig. 3, while results for *m/z* 29 ($C_2H_5^+$), 27 ($C_2H_3^+$), 39 ($C_3H_3^+$), and 67 ($C_5H_7^+$) are shown in Fig. 4. All of the reactive channels presented in Figs. 3 and 4 have cross sections that are weakly dependent of the methyl cation internal excitation in the explored photon energy range. Two exceptions are presented by channels leading to $C_2H_3^+$ and $C_3H_3^+$ (Fig. 4), for which cross sections are somehow constant in the range 9.8 eV–10.3 eV, and then they rise with the photon energy. Such behaviour is consistent with the opening of new reactive channels at higher photon energies. It is to be noted that the same two channels are observed to be favored by an increase in the collision energy (see Fig. 2), thus speaking for a requirement

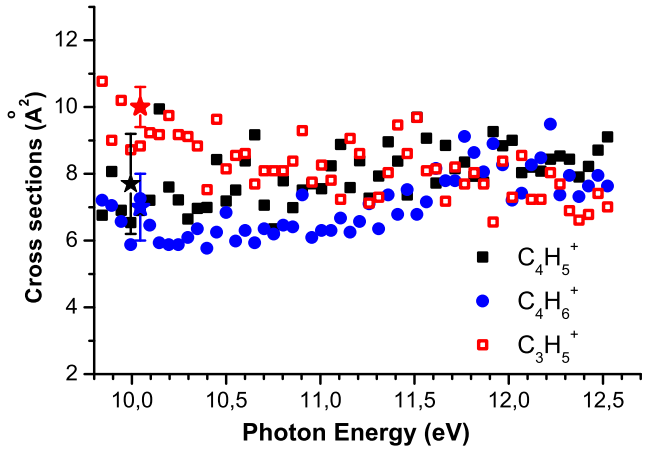

FIG. 3. Cross sections for the generation of the indicated ionic products formed in the reaction of mass-selected CH_3^+ with 2-butyne as a function of the photon energy used to ionise the $CH_3^\bullet$ precursor. The collision energy in the CM frame is fixed at about 0.3 eV. The star symbols indicate data obtained by measuring absolute cross sections values as a function of collision energy, at fixed photon energies (only the datapoint corresponding to E_{CM} = 0.3 eV is reported).

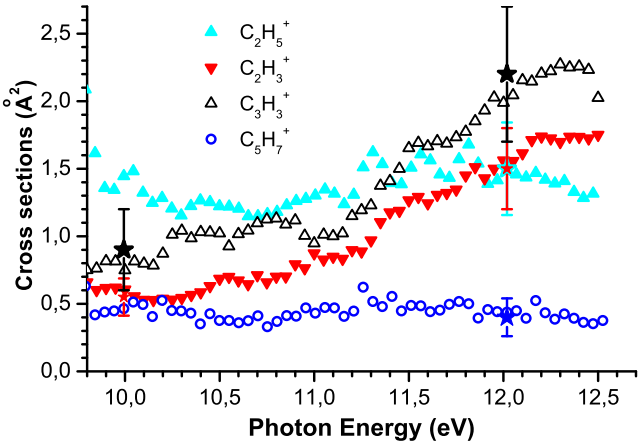

FIG. 4. Cross sections for the generation of the indicated ionic products formed in the reaction of mass-selected CH_3^+ with 2-butyne as a function of the photon energy used to ionise the $CH_3^\bullet$ precursor. The collision energy in the CM frame is fixed at about 0.3 eV. The star symbols indicate data obtained by measuring absolute cross sections values as a function of collision energy, at fixed photon energies (only the datapoint corresponding to E_{CM} = 0.3 eV is reported).

of a certain amount of internal or kinetic energy to overcome reaction barriers or unfavourable thermochemistry.

In addition to data taken in the *reaction monitoring mode*, product cross sections for reactions (1)–(7) have also been measured as a function of the collision energy at two fixed photon energies of 10 and 12 eV, see Figs. 5 and 6. BRs measured at 10 and 12 eV photon energies, at a collision energy E_{CM} ~ 0.3 eV and but-2-yne pressure ~2.1×10^{-4} mbar, are reported in Table III. For the determination of BRs, the same considerations previously reported in the discussion of Table II are valid. It is important to note that at 10 eV photon energy, the CH_3^+ parent ions are produced with essentially no excitation (mean vibrational energy smaller than 0.16 eV) and that at 12 eV photon energy, they are partially vibrationally excited with a mean energy of about 0.6 eV.[57] BRs obtained at 12 eV photon energy are identical, within the error bars, to data from the Trento experiment, and this is an indication that some internal excitation of the CH_3^+ cation is present in the dissociative

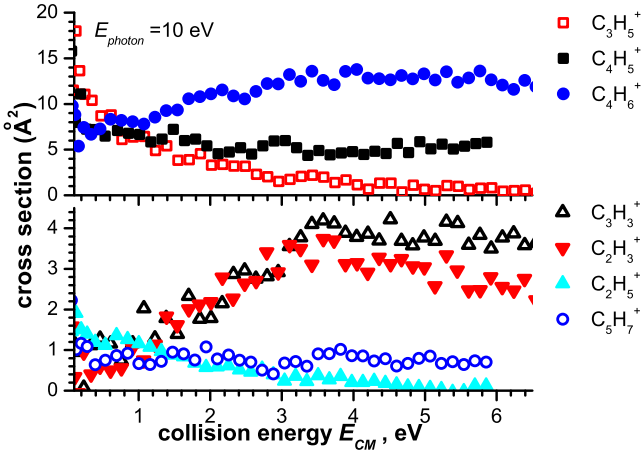

FIG. 5. Absolute cross sections as a function of collision energy for the generation of the indicated products from the reaction of mass-selected CH_3^+ with 2-butyne. The photon energy used to ionise the $CH_3^\bullet$ precursor is 10 eV.

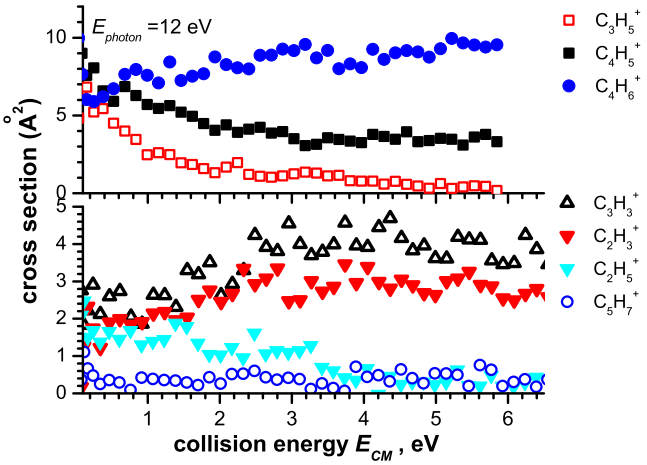

FIG. 6. Absolute cross sections as a function of collision energy for the generation of the indicated products from the reaction of mass-selected CH_3^+ with 2-butyne. The photon energy used to ionise the $CH_3^\bullet$ precursor is 12 eV.

electron ionization of acetone employed in the ion source of the Trento GIB-MS.

In the rest of this section, trends in the cross sections as a function the photon energy and collision energy for the various products are described in detail, starting from the most abundant products.

1. Products $C_4H_5^+$ (m/z 53) and $C_4H_6^{\bullet+}$ (m/z 54)

Products $C_4H_5^+$ and $C_4H_6^{\bullet+}$ are among the three most abundant channels (Table III), in agreement with what is already observed in Trento (Table II). For both products, cross sections as a function of the photon energy (Fig. 3), although data are quite scattered, are practically flat in the explored photon energy range. For the $C_4H_5^+$ product, cross sections as a function of the collision energy measured at 10 and 12 eV photon energies (black filled squares in Figs. 5 and 6, respectively) show a rather similar trend, namely, a slight decrease with increasing collision energy in the range 0 eV–2 eV, followed by a constant trend at high E_{CM}. This trend is in agreement with data taken in Trento (black filled squares in Fig. 2). Hence, the experimental evidence is that the internal energy of the parent cation does not affect the reaction probability, while there is a negative but moderate dependence on the kinetic energy.

TABLE III. Branching ratios for the formation of the main product channels observed upon reaction of CH_3^+, formed via photoionization of $CH_3^\bullet$ radicals at 10 and 12 eV photon energies, with but-2-yne (at a pressure of 2.1×10^{-4} mbar) and collision energy E_{CM} = 0.3 eV.

m/z	Ion	Branching ratios (%)–10 eV	Branching ratios (%)–12 eV
27	$C_2H_3^+$	2.6 ± 1.3	5.4 ± 0.8
29	$C_2H_5^+$	5.0 ± 1.1	6.0 ± 1.0
39	$C_3H_3^+$	2.1 ± 1.6	6.5 ± 1.1
41	$C_3H_5^+$	30 ± 6	23 ± 5
43	$C_3H_7^+$	n.d.	2.2 ± 1.0
53	$C_4H_5^+$	28 ± 5	24 ± 4
54	$C_4H_6^{+\bullet}$	31 ± 5	31 ± 4
67	$C_5H_7^+$	1.8 ± 0.4	1.7 ± 0.3

For the charge transfer product $C_4H_6^{\bullet+}$, cross sections as a function of the collision energy measured at 10 and 12 eV photon energies (blue filled circles in Figs. 5 and 6, respectively) show a slow rise with E_{CM}, similar to what is observed in Trento (blue filled circles in Fig. 2). In this case also, experiments indicate that the internal energy of CH_3^+ does not affect the reaction probability at E_{CM} = 0.3 eV (Fig. 3); however, the relative increase of the cross section with collision energy is clearly more pronounced at 10 eV photon energy than at 12 eV. The positive dependence on the collision energy is at odds with what it would normally be expected for an exoergic reaction. However, the dynamics of a charge transfer process is dictated by the position and the nature of the crossing between two diabatic potential energy surfaces and by the vibrational wavefunction overlaps (*Franck-Condon factors*). It might be possible here that the formation of vibrationally excited levels are more favored than the formation of ground state levels and, as the exothermicity (0.26 eV) of the charge transfer is small, this would explain the dependence observed with E_{CM}.[97] Finally, the fact that cross sections (for both $C_4H_5^+$ and $C_4H_6^{\bullet+}$ formations) do not decrease at high collision energies, but remain practically constant up to the highest energies explored in this study, is an indication that such channels are formed via a direct hydride (H^-) or electron transfer process rather than via the formation of a collision complex.

2. Product $C_3H_5^+$ (m/z 41)

Product $C_3H_5^+$ is the third most abundant reaction channel [BR = 23(5)% at 12 eV photon energy, Table III], in agreement with what is already observed in Trento [BR = 22.5 ± 4.6%, Table II]. Cross sections as a function of the photon energy (open red squares in Fig. 3), despite the large scattering of the data, show a slight decrease with increasing photon energy, which maybe due to the competition with other channels opening at higher E_{phot}. Cross sections as a function of the collision energy measured at 10 and 12 eV photon energies (open red squares in Figs. 5 and 6, respectively) are largest at the smallest reachable collision energies and then decrease rapidly when E_{CM} is increased. A similar trend is observed in the data taken in Trento (open red squares in Fig. 2) and it is an indication that the mechanism leading to $C_3H_5^+$ formation involves the decomposition of a long-lived collision complex with the release of C_2H_4.

3. Product $C_2H_5^+$ (m/z 29)

The ethyl cation $C_2H_5^+$ is one of the minor channels of the title reaction, with a BR = 6.0 ± 1.0% at 12 eV photon energy (Table III), in agreement with what is already observed in Trento [BR = 7.2 ± 2.0%, Table II]. Cross sections as a function of the photon energy (filled cyan triangles in Fig. 4), despite the large scattering of the data, are practically flat in the explored photon energy range. Cross sections as a function of the collision energy measured at 10 and 12 eV photon energies (filled cyan triangles in Figs. 5 and 6, respectively) show a similar decrease with increasing collision energy, in agreement with data taken at Trento (filled cyan triangles in Fig. 2). Hence, the experimental evidence is that the internal energy of the parent cation does not affect the reaction probability, while there is a negative but moderate dependence on the kinetic energy, speaking in favor of a complex mediated reaction mechanism.

4. Products $C_2H_3^+$ (m/z 27) and $C_3H_3^+$ (m/z 39)

Products $C_2H_3^+$ and $C_3H_3^+$ are minor channels (BRs in Tables II and III). They present a different dependence of the cross sections as a function of the photon energy with respect to the other products discussed so far, namely, a practically flat trend at low photon energies (in the range 9.8 eV–10.3 eV) followed by an increase with E_{phot} at photon energies higher than a certain threshold value. In the case of $C_2H_3^+$ (red filled triangles in Fig. 4), cross sections are constant, but non zero, up to about 10.3(1) eV and present quite a regular rise afterwards. In the case of $C_3H_3^+$ (open black triangles in Fig. 4), the rise of the cross section with E_{phot} is estimated at about 10.2(1) eV, and a linear rise is observed afterwards, with an increase of the slope above about 11.1 eV photon energy.

For both $C_2H_3^+$ and $C_3H_3^+$ channels, cross sections as a function of the collision energy measured with low internal excitation of the parent (i.e., at E_{phot} = 10 eV, red filled and open black triangles in Fig. 5, respectively) are very small (practically zero for $C_3H_3^+$) at the lowest collision energy, and then they rise with increasing E_{CM}, as expected for channels that require overcoming an energy barrier. Hence, the experimental evidence is that both kinetic and internal energies are efficient in favoring the production of $C_3H_3^+$ and $C_2H_3^+$. When some internal energy is placed into the CH_3^+ reagent (i.e., when the photon energy is increased to 12 eV, see red filled and open black triangles in Fig. 6 for $C_2H_3^+$ and $C_3H_3^+$, respectively), cross sections show an increase by a factor 2 to 3 at low collision energies (below 1 eV). The trend with increasing E_{CM} is similar to the 10 eV photon energy data: cross sections increase with E_{CM}, although the relative increase is smaller than at 10 eV, because some extra energy is provided to the reacting couple in the form of internal energy of the methyl cation. Data show that internal energy is more efficient than kinetic energy in promoting the formation of $C_2H_3^+$ and $C_3H_3^+$ species: when CH_3^+ has ~0.6 eV in vibrational excitation (data in Fig. 6), cross sections for the formation of $C_2H_3^+$ and $C_3H_3^+$ amount to 2-3 Å^2, to obtain similar cross sections when no internal energy is given to CH_3^+ (data at 10 eV, Fig. 5), collision energies larger than 2 eV should be employed.

5. Product $C_5H_7^+$ (m/z 67)

Despite being a minor channel (BR < 2%, see Tables II and III), the formation of $C_5H_7^+$ from the title reaction is of particular relevance because it is the only product of condensation with the formation of new C—C bonds and a mass increase with respect to the reagent masses. Hence, it can be a viable pathway in the synthesis of complex organic species, as it will be discussed in Sec. VI. To ensure that the signal at *m/z* 67 is not due to secondary reactions its pressure dependence was carefully checked and compared with that of *m/z* 53, 54, and 93: the dependence was found compatible with the occurrence of a primary process giving $C_5H_7^+$. Cross sections as a function of the photon energy (open blue circles in Fig. 4), despite the significant scattering of the data, are practically flat

in the explored photon energy range. Cross sections measured at 10 and 12 eV photon energies show no sizeable dependence on the collision energy (open blue circles in Figs. 5 and 6, respectively), and a similar trend is observed for the data taken in Trento (open blue circles in Fig. 2). Hence, the experimental evidence is that neither internal energy of the parent cation nor collision energy has a sizeable effect on the reaction probability.

V. THEORETICAL RESULTS AND DISCUSSION

To shed light on the formation mechanisms of the ionic products observed in both experiments at Trento and SOLEIL synchrotron, high level (CCSD(T)/CBS) electronic structure calculations of the most relevant stationary points on the potential energy hypersurface have been carried out. Attention was focused on the products corresponding to peaks at *m/z* 67, 54, 53, 41, 39, 29, and 27, which will be discussed separately in the following. The overall energy profile is shown in Fig. 7, and the experimental and calculated energies of the final product channels have been given in Table I. A couple of CCSD/cc-pVTZ optimizations (structure **6** and TS **6-7**) were carried out for comparison with the M06-2X geometries. The maximum difference for bond lengths was 0.02 Å (1%) and <4° (~3%) for angles. Despite the limited extent of the comparison, the small geometrical variations support the accuracy and reliability of the M06-2X geometries and the validity of our choice of theoretical methodology. In fact, CCSD(T) optimizations, in spite of a much higher computational cost, would have not provided any additional insight. The figures with CCSD and M06-2X optimized parameters are reported in the supplementary material.

A. Products $C_4H_6^{\bullet+}$ (*m/z* 54), $C_4H_5^+$ (*m/z* 53), and $C_2H_3^+$ (*m/z* 27)

The step (**0-1**) is a simple charge transfer leading to a $CH_3CCCH_3^{\bullet+}$ radical cation maintaining the structure of the corresponding but-2-yne neutral: formally, one electron is transferred from but-2-yne to the methyl cation, as exemplified by reaction (2), exoergic by 6.8 kcal mol^{-1} (0.3 eV).

The step (**0-3**) is a formal hydride abstraction from but-2-yne to the methyl cation, bringing to methane plus but-2-yn-1-yl cation (**3** in Scheme 1), i.e., reaction (1). The reaction occurs without any barrier on the potential energy surface and it is exoergic by 57.2 kcal mol^{-1} (2.48 eV). The exothermic nature of the step and the fact that the mechanism does not involve the formation of an intermediate complex is consistent with the experimental results, in particular with the negative but moderate dependence of the cross sections on the collision energy.

Further evolution of the $C_4H_5^+$ isomer corresponding to structure **3** via intermediate **4** leads to the vinyl cation $[CH_2CH]^+$ plus ethyne (**5** in Scheme 1). We note in passing that the $C_4H_5^+$ potential energy surface was also studied by Cunje *et al.* at the HF and MP2 levels.[86,98] Hence, our calculations propose that the $[CH_2CH]^+$ product is formed via the overall endoergic reaction (6a) (see Table I). We note that although channels (6b) and (6c) are exoergic, we have not been able to identify a viable pathway leading to the formation of C_3H_6 isomers as counter-fragments of the $[CH_2CH]^+$ product. Our experimental results are consistent with calculations: in fact, the experimental threshold observed at 10.3(1) eV photon energy (Fig. 4) is in good agreement with the calculated endothermicity for process (6a) ($\Delta_r H° = 0.44$ eV, Table I). The observation of constant but non-zero cross sections below the appearance threshold can be reconciled taking into account the mean collision energy, $E_{CM} \sim 0.3$ eV, and the kinetic energy spread of the primary CH_3^+ beam, having a FHWM (about 0.5–0.6 eV in the CM frame, see Sec. IV) of the same order of magnitude of the endothermicity for process (6a). In the data as a function of the collision energy (Fig. 5) when no internal energy is stored in the parent cation, a clear increase is observed in the cross sections at collision energies above 0.8 eV, in line with the predicted endothermicity, and low but non zero values are measured below these energies due to the kinetic energy spread.

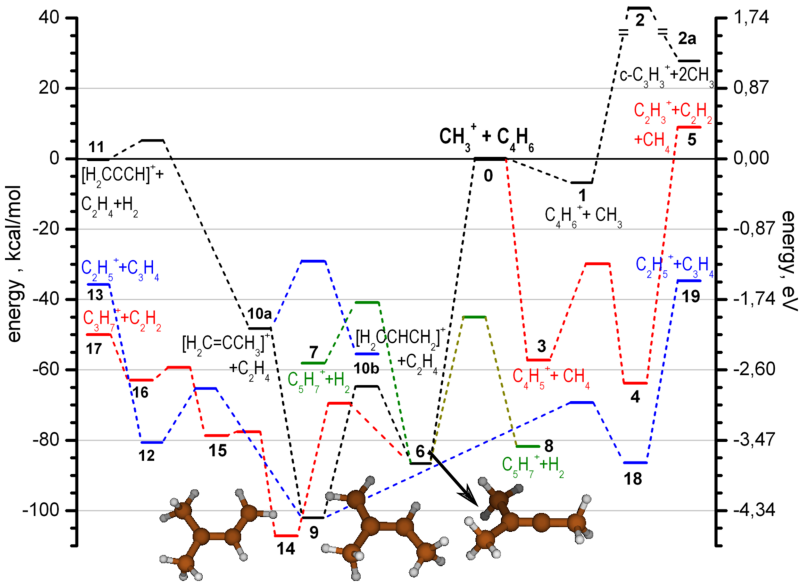

FIG. 7. Scheme of the most relevant reaction pathways for the title reaction. Energies (E_{ZPE}) are computed as detailed in the text. Note that the energy of structure **2** (97.6 kcal mol^{-1}) is out of scale. The optimized geometries of addition complexes corresponding to structures **6**, **9**, and **14** are also indicated. The experimental and calculated energies of the final product channels have been summarized in Table I.

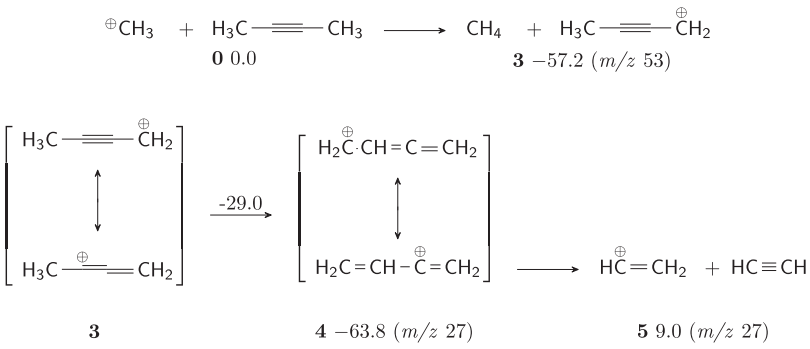

SCHEME 1. Formation of $C_4H_5^+$ (*m/z* 53) and $C_2H_3^+$ (*m/z* 27): energies are given in kcal mol^{-1}. The zero energy value is identified with the reactants' energy so that the reported energies refer to $\Delta_r E_{ZPE}$ values of Table I. Numbers in bold are labels for the different structures, as reported in Fig. 7.

B. Products $C_5H_7^+$ (*m/z* 67) and $C_3H_5^+$ (*m/z* 41)

The electrophilic CH_3^+ addition to but-2-yne generates an intermediate 86.6 kcal mol^{-1} more stable than the reactants (pathway **0** → **6** in Scheme 2). $C_5H_7^+$ is produced by H_2 loss from such an intermediate, via reaction (7). Depending on which methyl group is involved (blue or red hydrogens, in Scheme 2), two different isomers can be obtained: the linear 3-methyl-1-butyl cation (structure **7**) and the 1,2-dimethyl cyclopropyl cation $CH_3C_3HCH_3$ (structure **8**). The H_2 loss barriers for the two competitive reactions (**6** → **8** and **6** → **7**) are not too dissimilar but the isomer on the left (**8**) is more stable than **7** by about 23.7 kcal mol^{-1} (1.03 eV). Because of the low pressure at which our experiments are performed, and therefore the low collisional frequency, it is reasonable to assume that the system is not at the thermal equilibrium. The excess of rovibrational energy would allow it to easily overcome both barriers and consequently both isomers can form.

Alternatively, structure **6** can evolve into a very stable intermediate (**9** in Scheme 2) that opens the way to other experimentally detected species at *m/z* 41 ($C_3H_5^+$), *m/z* 39 ($C_3H_3^+$), and *m/z* 29 ($C_2H_5^+$), whose formation pathways are described in the following.

Structure **9** can rearrange into the prop-1-en-2-yl cation ($C_3H_5^+$ *m/z* 41) plus ethene C_2H_4 (structure **10a**). This channel has been indicated as reaction (3b) and its overall exoergicity is −48.3 kcal mol^{-1} (−2.10 eV). The $[CH_2{=}CCH_3]^+$ cation could isomerise to a more stable allyl cation $[CH_2CHCH_2]^+$ (−55.5 kcal mol^{-1}), with an energy barrier for H migration of

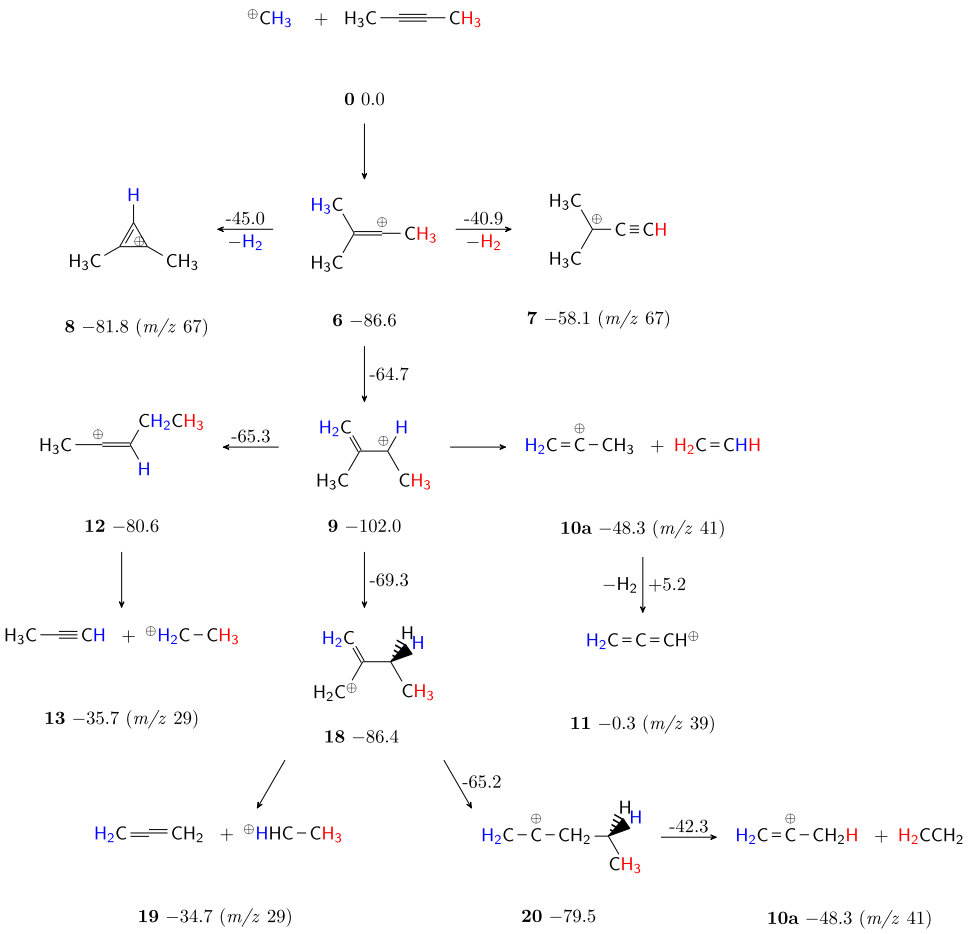

SCHEME 2. Formation mechanism of $C_5H_7^+$, $C_3H_5^+$, $C_3H_3^+$, and $C_2H_5^+$: energies are given in kcal mol^{-1}. The zero energy value is identified with the reactants' energy so that the reported energies refer to $\Delta_r E_{ZPE}$ values of Table I. Numbers in bold are labels for the different structures, as reported in Fig. 7.

19.1 kcal mol^{-1} (structure **10b**, not reported in Scheme 2 but shown in Fig. 7). Hence, also reaction (3a) is overall exoergic (by −2.41 eV) and it presents only submerged barriers. As a consequence, the observed product at *m/z* 41 could be either $[CH_2{=}CCH_3]^+$ or $[CH_2CHCH_2]^+$. We note in passing that the calculated energy difference between the two $C_3H_5^+$ isomers as well as the barrier for isomerization are in perfect agreement with the experimental values reported in the work of Holmes *et al.*[84] Another possibility to obtain structure **10a** from rearrangements of **9** is proposed in Scheme 2 (via intermediates **18** and **20**). However, due to the presence of three transition states, we expect that reaction (3b) will mostly proceed from structure **9** via the direct pathway **9** ⟶ **10a**.

Theoretical calculations predict that the formation of $C_3H_5^+$ and $C_5H_7^+$ is occurring via a complex-mediated mechanism going via the stable structure **6** (see Scheme 2) and presenting only submerged barriers afterwards. Measured cross-sections as a function of the collision energy for the $C_3H_5^+$ product are indeed consistent with the proposed mechanism, showing a marked decrease with increasing E_{CM} (see open red squares in Figs. 2, 5, and 6). On the contrary, the collision energy dependence for $C_5H_7^+$ is practically flat (open blue circles in Figs. 2, 5, and 6). In addition, $C_3H_5^+$ and $C_5H_7^+$ products have very different branching ratios: while $C_3H_5^+$ is one of the three most abundant products [BR is 22.5 ± 4.6% in Trento], $C_5H_7^+$ is a minor channel (BR ≤ 2%). Such findings could be reconciled with the proposed pathway having structure **6** in common, if the "rate determining step" is not related to the formation of adduct **6**. In fact, even though structure **7** or **8** (giving $C_5H_7^+$ in any of the two isomers) is more stable than structure **10a** ($[CH_2{=}CCH_3]^+$ plus ethane), the calculated energy barriers for H_2 loss from **6** (45.7 kcal mol^{-1} and 41.6 kcal mol^{-1} to give **7** and **8**, respectively) are consistently higher than the barrier for isomerization of **6** into **9** (21.9 kcal mol^{-1}). Hence, it is expected that most of the reactive flux reaching **6** will be channeled into the formation of **9** from which the abundant product $C_3H_5^+$ is subsequently formed. The high barriers present towards decomposition of **6** into $C_5H_7^+$ plus H_2 imply an increasing probability for this step with increasing E_{CM}. Then, as the cross section is proportional to the product of the probability of the barrierless and exothermic formation of adduct **6** (strongly decreasing with collision energy) by the probability of decomposition into products, it might explain the rather flat trend observed for $C_5H_7^+$ cross sections as a function of the collision energy.

C. Products $C_3H_3^+$ (*m/z* 39) and $C_2H_5^+$ (*m/z* 29)

The loss of an H_2 molecule from the prop-1-en-2-yl cation $[CH_2{=}CCH_3]^+$ (**10a**) leads to a propargyl cation $[HCCCH_2]^+$ (**11**), with an energy barrier of 53.5 kcal mol^{-1} [reaction (5f), Scheme 2]. Although the process is practically thermoneutral (exoergicity −0.3 kcal mol^{-1}, i.e., −0.01 eV), it presents an energy barrier at 5.2 kcal mol^{-1}(0.23 eV) relative to reagents. Incidentally we note that propargyl is one of the four known $C_3H_3^+$ isomers,[99,100] the most stable being the cyclopropenyl cation c—$C_3H_3^+$. However formation of the latter (structure **2a**) is energetically daunting since it requires to go via an intermediate (structure **2**) having an endothermicity of 97.6 kcal mol^{-1}, i.e., more than 4 eV (see details of our calculations in the supplementary material). Such enormous endothermicity makes this pathway unfeasible under our experimental conditions, as well as at the low temperatures of Titan's atmosphere.

For the sake of completeness, pathways for the formation of the fragment at *m/z* 39 (in any of its isomeric forms) in association with the neutral counter-fragment C_2H_6 have also been searched, but none were found. Therefore, channels (5b), (5e), and (5h) (see Table I) are not operative for the title reaction. Channel (5c) can also be excluded since the isomerization of the propargyl cation $[HCCCH_2]^+$ into the more stable cyclic isomer is hampered by a barrier of 85.2 kcal mol^{-1} (3.7 eV) according to our calculations.

Our experimental results for $C_3H_3^+$ formation are compatible with the proposed mechanism for reaction (5f): cross sections as a function of the photon energy (see Fig. 4) present a step-like increase at 10.2(1) eV (i.e., about 0.3 eV higher than threshold for the formation of the CH_3^+ parent), followed by the linear rise. The calculated kinetic energy barrier for H_2 loss from structure **10a** (0.23 eV) is slightly lower, but anyhow compatible, with the observed experimental threshold. As already mentioned for the $[CH_2CH]^+$ channel, the observation of constant but non-zero cross sections below the appearance threshold is due to the mean kinetic energy of the primary CH_3^+ beam and its spread, which is of the same order of magnitude of the energy barrier for the process (5f). The observed change of slope in the cross section at about 11.1 eV photon energy (i.e., about 1.2 eV higher in energy than the ionization energy of the $CH_3^\bullet$ radical) could be related to the increase in the mean internal energy of the CH_3^+ cation that is observed to start around 11.0 eV.

The mechanism bringing to the ethyl cation $C_2H_5^+$ plus propyne (**13**) goes from **9** via intermediate **12** and involves complicated rearrangements as detailed in Scheme 2 and in the supplementary material. The overall reaction (4a) has an exoergicity of −35.7 kcal mol^{-1} (−1.55 eV) and only presents submerged barriers. An alternative mechanism for the production of $C_2H_5^+$ plus a different C_3H_4 isomer (allene, $CH_2{=}C{=}CH_2$) as counter-fragment goes via the pathway **9** → **18** → **19**. The overall process (4b) is exoergic by −34.7 kcal mol^{-1} (−1.51 eV). Due to their very similar exoergicities and the exclusive presence of submerged barriers, channels (4a) and (4b) are both possible under our experimental conditions. Calculations compare well with the experimental findings for the product at *m/z* 29: cross sections show a decrease with increasing E_{CM} (see Figs. 2 and 5) as expected from exothermic channels stemming from the barrierless formation and decomposition of an addition complex between reactants. Formation of $C_2H_5^+$ is a minor reaction channel, with a BR consistently smaller [7.2 ± 2.0% in Trento and 6.0 ± 1.0% at Soleil with 12 eV photon energy, see Tables II and III] than the previously described $C_3H_5^+$, despite the fact that both products stem from the same intermediate **9** via overall exothermic mechanisms. Nonetheless, while the latter can form via the direct and irreversible decomposition of **9** into **10**, the former requires overcoming at least one transition state, either in going from **9** to **18** or in going from **9** to **12**, with the additional possibility of going back easily to **9**.

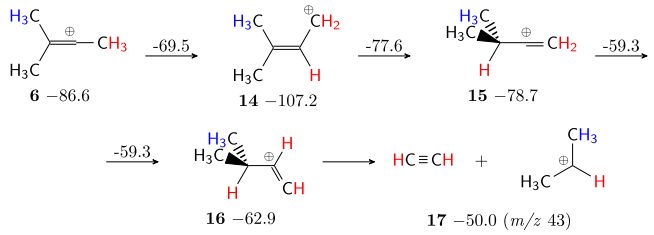

SCHEME 3. Formation mechanism of $C_3H_7^+$: energies are given in kcal mol^{-1}. The zero energy value is identified with the reactants' energy so that the reported energies refer to $\Delta_r E_{ZPE}$ values of Table I. Numbers in bold are labels for the different structures, as reported in Fig. 7.

D. Product $C_3H_7^+$ (*m/z* 43)

A small amount of signal is detected, in the Trento experiment, at *m/z* 43 (even at the lowest C_4H_6 pressure of 6.4 × 10^{-7} mbar) and it is assigned as the $C_3H_7^+$ cation, with a BR = 1.4(7)% (Table II). The collision energy dependence of the cross section for *m/z* 43 product is quite similar to that for *m/z* 41, showing a sharp decrease with increasing E_{CM}. In the SOLEIL experiment, a small peak at *m/z* 43 is visible, when 12 eV photons are employed, with a similar BR [2.2 ± 1.0%, see Table III]. The $C_3H_7^+$ cation could form, in association with C_2H_2 as counter-fragment, via the bimolecular process (8), which is exothermic by about 2 eV if the $C_3H_7^+$ ion has the structure of the 2-propyl cation (see Table I). We have explored theoretically such processes, and a viable mechanism for channel (8) was found, as described in Scheme 3.

The proposed mechanism entails the formation, series of rearrangements and decomposition of the already mentioned complex **6** between CH_3^+ and but-2-yne, in a process that is overall exoergic by 50 kcal mol^{-1} (2.19 eV) and presents only submerged barriers. Such a mechanism is consistent with the observed collision energy dependence of the cross sections and with the small BR observed for the $C_3H_7^+$ channel. In fact, the series of 1,2 H shifts rearrangements stemming from **6** could be responsible for the low amount of reactive flux following the pathway **6** ⟶ **14** ⟶ **15** ⟶ **16** ⟶ **17** (see Scheme 3). On the other hand, the absence of signal at *m/z* 43 in the SOLEIL experiment at 10 eV photon energy might be ascribed to low sensitivity since the branching ratio of this product is very small.

VI. CONCLUSIONS

The reactivity of methyl cations (CH_3^+) with but-2-yne (C_4H_6) has been investigated experimentally by guided ion beam mass spectrometric techniques using two different setups: in the Trento experiment, methyl cations are generated, with an uncontrolled amount of internal excitation, by electron ionization, while in the SOLEIL experiment, direct VUV photoionization with synchrotron radiation of methyl radicals—produced by a molecular beam pyrolysis source—is used to produce CH_3^+.

Primary product channels have been identified; branching ratios have been measured, as well as absolute reactive cross sections as a function of collision energy, in the thermal and hyperthermal energy ranges. The experimental studies are combined with a synergic theoretical investigation of possible reaction pathways, thus permitting a detailed understanding of the reaction mechanisms.

The two most abundant channels are charge transfer leading to the $CH_3CCCH_3^{\bullet+}$ radical cation (plus $CH_3^{\bullet}$) and hydride abstraction from but-2-yne to the methyl cation giving $C_4H_5^+$ (plus CH_4). Both processes occur via a direct mechanism and are exothermic and barrierless. Other channels are initiated by the electrophilic addition of the methyl cation to the triple bond of but-2-yne, leading to the formation of a complex (structure **6**) that can rearrange into two even more stable complexes (structures **9** and **14**).

The synthesis of $C_5H_7^+$ bears a special astrochemical interest because it is the only product of condensation with the formation of new C—C bonds. Hence, it can be a viable pathway for the synthesis of complex organic species, as put forward in the work of Ali *et al.*,[46] where the authors propose that the reactions of methyl cations with methylacetylene and dimethylacetylene in Titan's upper atmosphere might be responsible for the two couples of ions ($C_4H_7^+$, $C_4H_5^+$) and ($C_5H_9^+$, $C_5H_7^+$) observed in the mass spectra of Titan's ionosphere from the Ion and Neutral Mass Spectrometer on board of Cassini,[24–31]

$$CH_3^+ + CH_3CCH \longrightarrow CH_3C_3H_2^+ + H_2, \quad (9)$$

$$CH_3^+ + CH_3CCCH_3 \longrightarrow CH_3C_3HCH_3^+ + H_2. \quad (10)$$

Such predictions are based on an analogy with the bimolecular reaction of CH_3^+ with C_2H_2: kinetics[52–54] and dynamics studies,[55] supported by *ab initio* calculations of the potential energy surface,[56] indicate that the formation of $C_3H_3^+$ (plus H_2) is the only reaction channel, and both the cyclic and the linear $C_3H_3^+$ isomers are generated in the unimolecular decomposition of the short-lived collision complex $C_3H_5^+$. However it should be noted that in the C_2H_2 case, both the charge exchange and the hydride abstraction reactions (leading to $C_2H_2^+$ and C_2H^+, respectively) are strongly endothermic (by about 1.56 eV and 1.9 eV, respectively), hence "complex-forming" is the only viable reaction channel at low collision energies. When moving from C_2H_2 to CH_3CCH and CH_3CCCH_3, hydride abstraction and charge exchange reactions[101] become energetically possible and, since they are driven by long-range interactions, their occurrence draws reactive flux from the complex-mediated mechanism, thus decreasing the probability of reactions (9) and (10). Our study demonstrates that this is indeed the case for but-2-yne, for which production of $C_5H_7^+$ (plus H_2) is a minor channel having a BR < 2%. Another idea that is put forward in the work of Ali *et al.*[46] concerns the structures of the $C_4H_5^+$ and $C_5H_7^+$ species emerging from reactions (9) and (10). The authors' assumption that the potential energy characteristics of the system CH_3^+ + CH_3CCCH_3 should be similar to those for the CH_3^+ + C_2H_2 system (for which experiments show that with decreased reagents relative collision energy, the formation of the cyclopropenyl cation is favored with respect to the linear $[CH_2CCH]^+$ isomer[55]) led them to speculate that although both linear $[C(CH_3)_2CCH]^+$ and cyclic $CH_3C_3HCH_3^+$ isomers are accessible, the product branching ratios of cyclic to linear structures are strongly temperature dependent. Hence, as the temperature of the reactive system decreases down to

the expected temperatures of Titan's atmospheres or interstellar clouds, the kinetics of formation of the cyclic isomer is dominant. For the $CH_3^+ + C_2H_2$ system, calculations from the work of Lópes *et al.*[56] show that the cyclic isomer is approximately 27.4 kcal mol^{-1} more stable than the linear propargyl cation, and the barrier to the formation of c—$C_3H_3^+$ (plus H_2) is 45 kcal mol^{-1} below the energy of the reactants, while the corresponding barrier for the formation of the linear one $[CH_2CCH]^+$ (plus H_2) is only 24 kcal mol^{-1} below the energy of the reactants. Our calculations for the $CH_3^+ + CH_3CCCH_3$ system indicate that the cyclic dimethyl derivative is similarly more stable than the linear $[C(CH_3)_2CCH]^+$ one (by approximately 23.7 kcal mol^{-1}). However, the energy barriers for the formation of cyclic and linear species from structure **6** differ only by approximately 4.1 kcal mol^{-1}, with the cyclic isomer having the smaller barrier. On such a basis, we do not expect a strong preference for the formation of the cyclic isomer when the title reaction is occurring at low temperatures.

Our joint experimental and theoretical study describes for the first time the reaction of methyl cations with dimethyl substituted acetylene, with a complete understanding of the reaction mechanisms. They might contribute to improving models of hydrocarbon growth in gaseous environments fed by high energy sources, such as terrestrial and planetary ionospheres, cometary comae, the interstellar medium, as well as combustion systems and plasma setups for technological applications.

SUPPLEMENTARY MATERIAL

See supplementary material for the following: I. Corrections to BRs for secondary reactions. II. Comparison between geometries optimized with M06-2X/CC-pvTZ and CCSD/CC-pvtz methods. III. Additional product pathways for $C_3H_3^+$ isomers. IV. Details on the $C_2H_5^+$ production pathways. V. Geometries (Cartesian coordinates) and energetics of the optimized structures for reagents, products, intermediates, and transition states.

ACKNOWLEDGMENTS

This work was supported by the Department of Physics (UniTN), by the COST Action No. TD1308 (Origins and Evolution of Life on Earth and in the Universe) and the COST Action No. CM1401 (Our Astro-Chemical History). We thank the DESIRS beamline team, L. Nahon, G. Garcia, N. De Oliveira, and J.-F. Gil, for assistance during the synchrotron measurements and the technical staff of SOLEIL for running the facility. C.A. and C.R. acknowledge the synchrotron SOLEIL for the support to the associated CERISES setup since 2008 and subsistence expenses during beamtime periods. The Orsay group acknowledges support from the French program of planetology (PNP) and the RTRA "Triangle de la Physique" (contract RADICAUX and NOSTADYNE-2). J.Z. acknowledges support from the Czech Science Foundation (Grant No. 17-14200S). M.P. acknowledges support from the Ministry of Education, Youth and Sports (Grant No. LD14024).

[1] G. A. Olah, J. Am. Chem. Soc. **94**, 808 (1972).
[2] G. A. Olah, Angew. Chem., Int. Ed. Engl. **34**, 1393 (1995).
[3] V. R. Naidu, S. Ni, and J. Franzén, ChemCatChem **7**, 1896 (2015).
[4] T. Yuasa, S. Kadota, M. Tsue, M. Kono, H. Nomura, and Y. Ujiie, Proc. Combust. Inst. **29**, 743 (2002).
[5] T. Pedersen and R. C. Brown, Combust. Flame **94**, 433 (1993).
[6] C. De Bie, B. Verheyde, T. Martens, J. van Dijk, S. Paulussen, and A. Bogaerts, Plasma Processes Polym. **8**, 1033 (2011).
[7] C. De Bie, J. van Dijk, and A. Bogaerts, J. Phys. Chem. C **119**, 22331 (2015).
[8] R. Snoeckx, R. Aerts, X. Tu, and A. Bogaerts, J. Phys. Chem. C **117**, 4957 (2013).
[9] S. Petrie and D. K. Bohme, Mass Spectrom. Rev. **26**, 258 (2007).
[10] N. Indriolo, T. Oka, T. R. Geballe, and B. J. McCall, Astrophys. J. **711**, 1338 (2010).
[11] M. Agúndez and V. Wakelam, Chem. Rev. **113**, 8710 (2013).
[12] D. McElroy, C. Walsh, A. J. Markwick, M. A. Cordiner, K. Smith, and T. J. Millar, Astron. Astrophys. **550**, A36 (2013).
[13] E. Roueff, M. Gerin, D. C. Lis, A. Wootten, N. Marcelino, J. Cernicharo, and B. Tercero, J. Phys. Chem. A **117**, 9959 (2013).
[14] E. Roueff, EPJ Web Conf. **84**, 06004 (2015).
[15] V. Wakelam, J.-C. Loison, E. Herbst, B. Pavone, A. Bergeat, K. Béroff, M. Chabot, A. Faure, D. Galli, W. D. Geppert, D. Gerlich, P. Gratier, N. Harada, K. M. Hickson, P. Honvault, S. J. Klippenstein, S. D. L. Picard, G. Nyman, M. Ruaud, S. Schlemmer, I. R. Sims, D. Talbi, J. Tennyson, and R. Wester, Astrophys. J., Suppl. Ser. **217**, 20 (2015).
[16] W. D. Geppert and M. Larsson, Chem. Rev. **113**, 8872 (2013).
[17] M. Larsson, W. D. Geppert, and G. Nyman, Rep. Prog. Phys. **75**, 066901 (2012).
[18] D. Gerlich and G. Kaefer, Astrophys. J. **347**, 849 (1989).
[19] M. Kamińska, V. Zhaunerchyk, E. Vigren, M. Danielsson, M. Hamberg, W. D. Geppert, M. Larsson, S. Rosén, R. D. Thomas, and J. Semaniak, Phys. Rev. A **81**, 062701 (2010).
[20] N. Harada, E. Herbst, and V. Wakelam, Astrophys. J. **721**, 1570 (2010).
[21] M. Rubin, K. C. Hansen, T. I. Gombosi, M. R. Combi, K. Altwegg, and H. Balsiger, Icarus **199**, 505 (2009).
[22] Y. H. Kim and J. L. Fox, Icarus **112**, 310 (1994).
[23] Y. H. Kim, J. L. Fox, J. H. Black, and J. I. Moses, J. Geophys. Res.: Space Phys. **119**, 384, doi:10.1002/2013ja019022 (2014).
[24] R. H. Brown, J.-P. Lebreton, and J. H. Waite, *Titan from Cassini-Huygens* (Springer, Dordrecht, Netherlands, 2010).
[25] V. Vuitton, O. Dutuit, M. Smith, and N. Balucani, "Chemistry of titan's atmosphere," in *Titan: Interior, Surface, Atmosphere, and Space Environment*, Cambridge Planetary Science, edited by I. Müller-Wodarg, C. Griffith, E. Lellouch, and T. Cravens (Cambridge University Press, 2014), p. 224.
[26] J. H. Waite, Jr., H. Niemann, R. V. Yelle, W. T. Kasprzak, T. E. Cravens, J. G. Luhmann, R. L. McNutt, W.-H. Ip, D. Gell, V. De La Haye, I. Müller-Wordag, B. Magee, N. Borggren, S. Ledvina, G. Fletcher, E. Walter, R. Miller, S. Scherer, R. Thorpe, J. Xu, B. Block, and K. Arnett, Science **308**, 982 (2005).
[27] T. E. Cravens, I. P. Robertson, J. H. Waite, Jr., R. V. Yelle, W. T. Kasprzak, C. N. Keller, S. A. Ledvina, H. B. Niemann, J. G. Luhmann, R. L. McNutt, W.-H. Ip, V. De La Haye, I. Mueller-Wodarg, J.-E. Wahlund, V. G. Anicich, and V. Vuitton, Geophys. Res. Lett. **33**, L07105, doi: 10.1029/2005gl025575 (2006).
[28] J. H. Waite, Jr., D. T. Young, T. E. Cravens, A. J. Coates, F. J. Crary, B. Magee, and J. Westlake, Science **316**, 870 (2007).
[29] V. Vuitton, R. V. Yelle, and M. J. McEwan, Icarus **191**, 722 (2007).
[30] B. A. Magee, J. H. Waite, K. E. Mandt, J. Westlake, J. Bell, and D. A. Gell, Planet. Space Sci. **57**, 1895 (2009).
[31] J. Cui, R. V. Yelle, V. Vuitton, J. W. Waite, Jr., W. T. Kasprzak, D. A. Gell, H. B. Niemann, I. C. F. Müller-Wodarg, N. Borggren, G. G. Fletcher, E. L. Patrick, E. Raaen, and B. A. Magee, Icarus **200**, 581 (2009).
[32] G. Tinetti, Philos. Trans. R. Soc., A **372**, 20130077 (2014).
[33] T. S. Barman, Q. M. Konopacky, B. Macintosh, and C. Marois, Astrophys. J. **804**, 61 (2015).
[34] O. Venot, E. Hébrard, M. Agúndez, L. Decin, and R. Bounaceur, Astron. Astrophys. **577**, A33 (2015).
[35] K. J. Zahnle and M. S. Marley, Astrophys. J. **797**, 41 (2014).
[36] R. Hu and S. Seager, Astrophys. J. **784**, 63 (2014).
[37] U. Marboeuf, A. Thiabaud, Y. Alibert, N. Cabral, and W. Benz, Astron. Astrophys. **570**, A35 (2014).

[38] C. Bilger, P. Rimmer, and Ch. Helling, Mon. Not. R. Astron. Soc. **435**, 1888 (2013).
[39] M. R. Swain, P. Deroo, C. A. Griffith, G. Tinetti, A. Thatte, G. Vasisht, P. Chen, J. Bouwman, I. J. Crossfield, D. Angerhausen, C. Afonso, and T. Henning, Nature **463**, 637 (2010).
[40] M. R. Line, M. C. Liang, and Y. L. Yung, Astrophys. J. **717**, 496 (2010).
[41] K. E. Mandt, D. A. Gell, M. Perry, J. H. Waite, Jr., F. A. Crary, D. Young, B. A. Magee, J. H. Westlake, T. Cravens, W. Kasprzak, G. Miller, J.-E. Wahlund, K. Ågren, N. J. T. Edberg, A. N. Heays, B. R. Lewis, S. T. Gibson, V. de la Haye, and M.-C. Liang, J. Geophys. Res.: Planets **117**, E10006, doi:10.1029/2012je004139 (2012).
[42] T. Cravens, R. Yelle, J. Wahlund, D. Shemansky, and A. Nagy, "Composition and structure of the ionosphere and thermosphere," in *Titan From Cassini-Huygens* (Springer, The Netherlands, 2010), pp. 259–295.
[43] V. Vuitton, R. V. Yelle, and P. Lavvas, Philos. Trans. R. Soc., A **367**, 729 (2009).
[44] O. Dutuit, N. Carrasco, R. Thissen, V. Vuitton, C. Alcaraz, P. Pernot, N. Balucani, P. Casavecchia, A. Canosa, S. Le Picard, J.-C. Loison, Z. Herman, J. Žabka, D. Ascenzi, P. Tosi, P. Franceschi, S. D. Price, and P. Lavvas, Astrophys. J., Suppl. Ser. **204**, 20 (2013).
[45] V. D. L. Haye, J. H. Waite, Jr., T. E. Cravens, I. P. Robertson, and S. Lebonnois, Icarus **197**, 110 (2008).
[46] A. Ali, E. C. Sittler, Jr., D. Chornay, B. Rowe, and C. Puzzarini, Planet. Space Sci. **87**, 96 (2013).
[47] J. J. Fisher, G. K. Koyanagi, and T. B. McMahon, Int. J. Mass Spectrom. **195**, 491 (2000).
[48] V. G. Anicich, "An index of the literature for bimolecular gas phase cation-molecule reaction kinetics," Report JPL-Publ-03-19, 2003.
[49] S. Mark, C. Schellhammer, G. Niedner-Schatteburg, and D. Gerlich, J. Phys. Chem. **99**, 15587 (1995).
[50] C. Berg, W. Wachter, T. Schindler, C. Kronseder, G. Niedner-Schatteburg, V. E. Bondybey, and Z. Herman, Chem. Phys. Lett. **216**, 465 (1993).
[51] M. Fárník, Z. Dolejšek, Z. Herman, and V. E. Bondybey, Chem. Phys. Lett. **216**, 458 (1993).
[52] J. K. Kim, V. G. Anicich, and W. T. Huntress, Jr., J. Phys. Chem. **81**, 1798 (1977).
[53] V. G. Anicich, W. T. Huntress, Jr., and M. J. McEwan, J. Phys. Chem. **90**, 2446 (1986).
[54] A. Fiaux, D. L. Smith, and J. H. Futrell, Int. J. Mass Spectrom. Ion Phys. **25**, 281 (1977).
[55] D. M. Sonnenfroh and J. M. Farrar, J. Chem. Phys. **85**, 7167 (1986).
[56] R. López, J. A. Sordo, T. L. Sordo, and P. von Ragué Schleyer, J. Comput. Chem. **17**, 905 (1996).
[57] A. Lopes, C. Romanzin, B. K. Cunha de Miranda, I. Zymak, M. Žabka, J. Polášek, A. Cernuto, D. Ascenzi, and C. Alcaraz "Effects of collision energy and vibrational excitation of CH_3^+ cations on its reactivity with hydrocarbons: Methane as reagent partner" (unpublished).
[58] C. Alcaraz, C. Nicolas, R. Thissen, J. Žabka, and O. Dutuit, J. Phys. Chem. A **108**, 9998 (2004).
[59] P. Fathi, W. D. Geppert, A. Kaiser, and D. Ascenzi, Mol. Astrophys. **2**, 1 (2016).
[60] D. Ascenzi, N. Cont, G. Guella, P. Franceschi, and P. Tosi, J. Phys. Chem. A **111**, 12513 (2007).
[61] P. Franceschi, L. Penasa, D. Ascenzi, D. Bassi, M. Scotoni, and P. Tosi, Int. J. Mass Spectrom. **265**, 224 (2007).
[62] K. M. Ervin and P. B. Armentrout, J. Chem. Phys. **83**, 166 (1985).
[63] B. Cunha de Miranda, C. Romanzin, S. Chefdeville, V. Vuitton, J. Žabka, M. Polášek, and C. Alcaraz, J. Phys. Chem. A **119**, 6082 (2015).
[64] B. K. Cunha de Miranda, C. Alcaraz, M. Elhanine, B. Noller, P. Hemberger, I. Fischer, G. A. Garcia, H. Soldi-Lose, B. Gans, L. A. Vieira Mendes, S. Boyé-Péronne, S. Douin, J. Žabka, and P. Botschwina, J. Phys. Chem. A **114**, 4818 (2010).
[65] L. Nahon, N. de Oliveira, G. A. Garcia, J.-F. Gil, B. Pilette, O. Marcouillé, B. Lagarde, and F. Polack, J. Synchrotron Radiat. **19**, 508 (2012).
[66] B. Mercier, M. Compin, C. Prevost, G. Bellec, R. Thissen, O. Dutuit, and L. Nahon, J. Vac. Sci. Technol., A **18**, 2533 (2000).
[67] A. M. Schulenburg, C. Alcaraz, G. Grassi, and F. Merkt, J. Chem. Phys. **125**, 104310 (2006).
[68] A. Kramida, Y. Ralchenko, J. Reader, and NIST ASD Team, NIST Atomic Spectra Database (ver. 5.3), 2016.
[69] J. Roithová, D. Schröder, J. Loos, H. Schwarz, H.-C. Jankowiak, R. Berger, R. Thissen, and O. Dutuit, J. Chem. Phys. **122**, 094306 (2005).
[70] R. Parr and W. Yang, *Density-Functional Theory of Atoms and Molecules* (John Wiley and Sons, Inc., 1989), Vol. 3, p. 333.
[71] Y. Zhao and D. G. Truhlar, Theor. Chem. Acc. **120**, 215 (2007).
[72] Y. Zhao and D. G. Truhlar, J. Phys. Chem. A **112**, 1095 (2008).
[73] Y. Zhao and D. G. Truhlar, Acc. Chem. Res. **41**, 157 (2008).
[74] Y. Zhao and D. G. Truhlar, J. Chem. Theory Comput. **4**, 1849 (2008).
[75] R. A. Kendall, T. H. Dunning, Jr., and R. J. Harrison, J. Chem. Phys. **96**, 6796 (1992).
[76] D. E. Woon and T. H. Dunning, Jr., J. Chem. Phys. **98**, 1358 (1993).
[77] J. Li, A. B. Pacheco, K. Raghavachari, and S. S. Iyengar, Phys. Chem. Chem. Phys. **18**, 29395 (2016).
[78] S. Kozuch, Phys. Chem. Chem. Phys. **17**, 16688 (2015).
[79] R. Kalescky, W. Zou, E. Kraka, and D. Cremer, J. Phys. Chem. A **118**, 1948 (2014).
[80] A. Halkier, T. Helgaker, P. Jørgensen, W. Klopper, H. Koch, J. Olsen, and A. K. Wilson, Chem. Phys. Lett. **286**, 243 (1998).
[81] A. Halkier, T. Helgaker, P. Jørgensen, W. Klopper, and J. Olsen, Chem. Phys. Lett. **302**, 437 (1999).
[82] M. J. Frisch, G. W. Trucks, H. B. Schlegel, G. E. Scuseria, M. A. Robb, J. R. Cheeseman, G. Scalmani, V. Barone, G. A. Petersson, H. Nakatsuji, X. Li, M. Caricato, A. V. Marenich, J. Bloino, B. G. Janesko, R. Gomperts, B. Mennucci, H. P. Hratchian, J. V. Ortiz, A. F. Izmaylov, J. L. Sonnenberg, D. Williams-Young, F. Ding, F. Lipparini, F. Egidi, J. Goings, B. Peng, A. Petrone, T. Henderson, D. Ranasinghe, V. G. Zakrzewski, J. Gao, N. Rega, G. Zheng, W. Liang, M. Hada, M. Ehara, K. Toyota, R. Fukuda, J. Hasegawa, M. Ishida, T. Nakajima, Y. Honda, O. Kitao, H. Nakai, T. Vreven, K. Throssell, J. A. Montgomery, Jr., J. E. Peralta, F. Ogliaro, M. J. Bearpark, J. J. Heyd, E. N. Brothers, K. N. Kudin, V. N. Staroverov, T. A. Keith, R. Kobayashi, J. Normand, K. Raghavachari, A. P. Rendell, J. C. Burant, S. S. Iyengar, J. Tomasi, M. Cossi, J. M. Millam, M. Klene, C. Adamo, R. Cammi, J. W. Ochterski, R. L. Martin, K. Morokuma, O. Farkas, J. B. Foresman, and D. J. Fox, GAUSSIAN 16, Revision A.03, Gaussian, Inc., Wallingford CT, 2016.
[83] G. Schaftenaar and J. H. Noordik, J. Comput.-Aided Mol. Des. **14**, 123 (2000).
[84] J. Holmes, C. Aubry, and P. Mayer, *Assigning Structures to Ions in Mass Spectrometry* (CRC Press, 2006).
[85] NIST Chemistry WebBook, NIST standard reference Database, Number 69, National Institute of Standards and Technology, Gaithersburg, MD, 2015.
[86] A. Cunje, C. F. Rodriquez, M. H. Lien, and A. C. Hopkinson, J. Org. Chem. **61**, 5212 (1996).
[87] B. Ruscic, Active Thermochemical Tables (ATcT) values based on ver. 1.118 of the Thermochemical Network, 2015.
[88] S. T. Park, S. K. Kim, and M. S. Kim, J. Chem. Phys. **114**, 5568 (2001).
[89] T. Baer, J. Am. Chem. Soc. **102**, 2482 (1980).
[90] M. Polášek, E.-L. Zins, C. Alcaraz, J. Žabka, V. Křížová, L. Giacomozzi, P. Tosi, and D. Ascenzi, J. Phys. Chem. A **120**, 5041 (2016).
[91] C. J. Shaffer, D. Schröder, J. Roithová, E.-L. Zins, C. Alcaraz, J. Žabka, M. Polášek, and D. Ascenzi, Int. J. Mass Spectrom. **336**, 17 (2013).
[92] C. J. Shaffer, D. Schröder, C. Alcaraz, J. Žabka, and E.-L. Zins, ChemPhysChem **13**, 2688 (2012).
[93] C. Shaffer, D. Schröder, E.-L. Zins, C. Alcaraz, J. Žabka, and J. Roithová, Chem. Phys. Lett. **534**, 8 (2012).
[94] E.-L. Zins, P. Milko, D. Schröder, J. Aysina, D. Ascenzi, J. Žabka, C. Alcaraz, S. D. Price, and J. Roithová, Chem. - Eur. J. **17**, 4012 (2011).
[95] D. Ascenzi, J. Aysina, E.-L. Zins, D. Schröder, J. Žabka, C. Alcaraz, S. D. Price, and J. Roithová, Phys. Chem. Chem. Phys. **13**, 18330 (2011).
[96] D. Ascenzi, J. Roithová, D. Schröder, E.-L. Zins, and C. Alcaraz, J. Phys. Chem. A **113**, 11204 (2009).
[97] R. Candori, S. Cavalli, F. Pirani, A. Volpi, D. Cappelletti, P. Tosi, and D. Bassi, J. Chem. Phys. **115**, 8888 (2001).
[98] They took into account 14 different isomers and the transition structures for their interconversions. The most stable isomer was a methylcyclopropenyl cation and the energy difference between buta-1,3-dien-2-yl (**4**) and but-2-yn-1yl cation (**3**) was 10.0 and 5.4 kcal mol^{-1} at HF/6–31G(d,p) and MP2/6–311G(d,p), respectively. In this work, the difference is 6.5 kcal mol^{-1}, which is consistent with their results.
[99] L. Radom, P. C. Hariharan, J. A. Pople, and P. v. R. Schleyer, J. Am. Chem. Soc. **98**, 10 (1976).
[100] W.-K. Li and N. V. Riggs, J. Mol. Struct.: THEOCHEM **257**, 189 (1992).
[101] In the CH_3CCH case, charge exchange remains endothermic by about 0.5 eV, while hydride transfer leading to CH_4 plus CH_2CCH^+ (propargyl cation) is exothermic by about 1.9 eV.